

CS-Based HRRP Extraction Method for Through-Wall Detection

Fangfang Wang^{1, 2, *} and Tingting Qin¹

Abstract—Feature extraction is of significant importance for final results of the through-wall detection procedure. High resolution range profile (HRRP) is related to target reflectivity coefficients which can be used as a new feature for object detection. Compressive sensing (CS) is an emerging technique which enables a sparse signal to be recovered using much fewer measurements. This method can provide a novel way for achieving the HRRP since the target reflectivity coefficients are often known to be sparsely distributed in range cells. In this paper, after a set of input-output patterns that consist of target position and HRRP are obtained, through-wall detection problem is reformulated into a nonlinear regression one, which can be solved by support vector machine (SVM). Numerical simulations demonstrate that the prediction accuracy of target position is related to the number of range cells, the number of observations, and signal-to-noise ratio (SNR). Furthermore, the proposed method performs better than the one using signal amplitude as a feature in terms of smaller estimation error and shows better robustness against noise.

1. INTRODUCTION

Sensing through opaque medium obstacles such as walls and ground using ultra-wideband (UWB) signals is emerging as a powerful technology to support a variety of civilian and military applications [1]. Thus, through-wall detection is a research field of remote sensing which has many important applications in rescue and security [2].

There are several challenges in detecting objects behind a wall compared to the detection problem in free space. The main challenge in through-wall detection comes from the presence of the wall [3–5]. In addition, wall characteristics such as width, permittivity, and conductivity are unknown in most applications, which is another challenge for through-wall detection. Data-driven modelling (DDM) is a new approach in the area of machine learning which is based on analyzing the data about a system. Data-driven model is a good alternative to physics-based model for this problem when multiple data pairs containing the sensor output and the required object parameters are available. The characteristic of this DDM approach is its ability to capture the explicit knowledge of the physical behavior of the system.

Through-wall detection accuracy based on DDM is closely related to the feature that is extracted from the sensor output. Usually, the target signal received at each receiver antenna position of synthetic aperture radar (SAR) is not suitable for being treated as the feature directly even after wall clutter removal since it will lead to large amount of data. In order to alleviate processing bottleneck of high-speed data acquisition, storing, and transmission, it is inevitable to extract some statistical features (such as mean and variance) of the target signal received at each receiver antenna position. However, the statistical feature is an approximated one which will lose some information representing target characteristic. Besides, the amplitude of the target signal is also extracted as the feature. In [6, 7],

Received 26 April 2019, Accepted 19 July 2019, Scheduled 29 July 2019

* Corresponding author: Fangfang Wang (wangff@njupt.edu.cn).

¹ School of Electronic Science and Engineering, Nanjing University of Posts and Telecommunications, Nanjing 210003, China. ² State Key Laboratory of Millimeter Waves, Southeast University, Nanjing 211189, China.

a vector containing the largest amplitude of the signal received at each receiver antenna position is considered as an input of the support vector machine (SVM) model, and the target position is the output. However, this feature still cannot represent all characteristics of the target. To overcome these limitations, an alternative and innovative feature should be extracted for through-wall detection with high fidelity.

High resolution range profile (HRRP) is a feature which is successfully used in the classification and recognition of large targets (ships, aircraft, etc.) [8, 9]. HRRP represents the projection of target scattering centers on radar line of sight, and it is the coherent summation of complex echoes from target scatters in each range cell. HRRP contains the detailed target structure information, such as strength, size, and characteristic distribution of the target. Recent researches on SAR imaging show that the sparse reconstruction can achieve an HRRP with fewer pulses [10, 11]. Sparse representation is a signal processing technique that takes advantage of signal's sparsity, allowing signal to be recovered from a limited number of measurements with high probability by solving a convex optimization problem [12]. Compressive sensing (CS), a new branch of the sparse signal processing method, provides an efficient way of HRRP reconstruction with high accuracy and low side-lobe using far fewer observations [13, 14]. Therefore, CS provides a novel method for HRRP extraction.

In this paper, we first exploit CS theory to reconstruct the target's HRRP. With regard to the spatial sparsity of the radar scene, HRRP can be recovered even when the radar measurements are fewer. Experiment results show that HRRP can capture the important properties of radar returns. Then, a data-driven model is built up for through-wall detection with the knowledge of input and output pairs. Specifically, HRRP is treated as input and target's position as output. In this framework, through-wall detection is cast into a regression one which is solved by SVM.

The remainder of this paper is organized as follows. Section 2 firstly presents the signal model, and then CS is applied to extract the HRRP feature. After obtaining the pairs that consists of the target position and corresponding HRRP, through-wall detection problem can be recast as a regression one which is solved using SVM. In Section 3, numerical results for synthetic data are shown, and the performance of the proposed method is assessed in terms of accuracy, robustness, and compared with other methods. Finally, some conclusions and final remarks are made.

2. HRRP BASED THROUGH-WALL LOCALIZATION

2.1. Signal Model

Assume that N is the number of transceiver antenna positions and that M is the number of time samples at each antenna position. The transmitted waveform at each transceiver antenna position is a sinusoidal modulated Gaussian pulse, which is given by

$$E(t) = \sin(2\pi f_0 t) \exp \left[-\frac{4\pi(t_0 - t)^2}{\tau^2} \right] \quad (1)$$

here f_0 is the center frequency; the peak of the excitation pulse appears at t_0 ; and its spread is τ . Therefore, the m th sample of the target signal (after clutter suppression) at the n th antenna position from P targets can be expressed as

$$y(n, m) = \sum_{p=1}^P \sigma_p \sin(2\pi f_0 (t_m - 2r_{n,p}/c)) \exp \left[-\frac{4\pi(t_0 - (t_m - 2r_{n,p}/c))^2}{\tau^2} \right] \quad (2)$$

where σ_p is the reflectivity coefficient of the p th target, $r_{n,p}$ the range for the signal to travel between the n th antenna position and the p th target, and c the speed of light.

2.2. Feature Extraction

CS has brought a new paradigm in recovering a signal from lower dimensional measurements. In the application of CS, the signal is demanded to be sparse. In this paper, CS is applied to perform feature extraction of the target signal received at each transceiver antenna position separately. Assume that

$\mathbf{y}_n \in R^{M \times 1}$ is the target signal received at the n th transceiver antenna position which can be illustrated as

$$\mathbf{y}_n = [y(n, 1), y(n, 2), \dots, y(n, M)]^T \quad (3)$$

and $\boldsymbol{\theta}_n \in R^{I \times 1}$ is the HRRP at the n th transceiver antenna position

$$\boldsymbol{\theta}_n = [\theta_{n,1}, \theta_{n,2}, \dots, \theta_{n,I}]^T \quad (4)$$

where

$$\theta_{n,i} = \begin{cases} \sigma_p & r_i = r_{n,p} \\ 0 & \text{otherwise} \end{cases} \quad i = 1, 2, \dots, I, \quad p = 1, 2, \dots, P \quad (5)$$

Here, the target scene is divided into I ($I = \lceil r_w / \Delta r \rceil$) range cells, where $r_i \in \{i\Delta r | i = 1, 2, \dots, I\}$ represents the i th range cell, and $\lceil \cdot \rceil$ is the ceiling function. It should be noted that r_w is the maximum range that we are interested in, and Δr is the range resolution.

Then, the relationship between the target signal \mathbf{y}_n and the HRRP $\boldsymbol{\theta}_n$ is given by

$$\mathbf{y}_n = \boldsymbol{\Psi} \boldsymbol{\theta}_n \quad (6)$$

where $\boldsymbol{\Psi}$ is an $M \times I$ matrix whose (j, i) th element is

$$[\boldsymbol{\Psi}]_{ji} = \sin(2\pi f_0(t_j - 2r_i/c)) \exp\left[-\frac{4\pi(t_0 - (t_j - 2r_i/c))^2}{\tau^2}\right] \quad (7)$$

Note that HRRP $\boldsymbol{\theta}_n$ ($n = 1, \dots, N$) at each transceiver antenna position is different due to the diversity of the relative distance from the transceiver antenna position to the range cell position. In CS applications, the lower dimensional measurement $\tilde{\mathbf{y}}_n \in R^{Q \times 1}$ is acquired. The relation between the target signal \mathbf{y}_n and the measurement $\tilde{\mathbf{y}}_n$ is expressed as

$$\tilde{\mathbf{y}}_n = \boldsymbol{\Phi} \mathbf{y}_n = \boldsymbol{\Phi} \boldsymbol{\Psi} \boldsymbol{\theta}_n \quad (8)$$

where $\boldsymbol{\Phi}$ is a $Q \times M$ measurement matrix. Note that $\boldsymbol{\Phi}$ can be the same or different at each transceiver antenna position. The product of the measurement matrix $\boldsymbol{\Phi}$ and dictionary $\boldsymbol{\Psi}$ is denoted as

$$\mathbf{A} = \boldsymbol{\Phi} \boldsymbol{\Psi} \quad (9)$$

where \mathbf{A} is a $Q \times I$ matrix called sensing matrix.

The sparse HRRP $\boldsymbol{\theta}_n$ can be recovered from the solution of the following optimization problem

$$\hat{\boldsymbol{\theta}}_n = \arg \min \|\boldsymbol{\theta}_n\|_1 \text{ s.t. } \mathbf{A} \boldsymbol{\theta}_n = \tilde{\mathbf{y}}_n \quad (10)$$

where $\|\cdot\|_1$ is l_1 -norm such that $\|\boldsymbol{\theta}_n\|_1 = \sum_i |\theta_{n,i}|$. The problem given in Eq. (10) can be solved using orthogonal matching pursuit (OMP) [15]. The algorithm of OMP is shown below, and here $\boldsymbol{\alpha}_i$ is an atom of \mathbf{A} .

Input:

- $Q \times I$ sensing matrix \mathbf{A}
- Q -dimensional data vector $\tilde{\mathbf{y}}_n$
- The sparsity level k of the signal

Output:

- An estimate $\hat{\boldsymbol{\theta}}_n \in R^{I \times 1}$ for the signal

Procedure:

- 1) Initialize the residual $\mathbf{r}_0 = \tilde{\mathbf{y}}_n$, the index set $\boldsymbol{\Lambda}_0 = \emptyset$, the sensing matrix $\mathbf{A}_0 = \emptyset$, and the iteration step $t = 1$.
- 2) Find the index λ_t that solves the following optimization problem

$$\lambda_t = \arg \max_{j=1,2,\dots,I} |\langle \mathbf{r}_{t-1}, \boldsymbol{\alpha}_j \rangle| \quad (11)$$

- 3) Augment the index set and the matrix of the chosen atom: $\boldsymbol{\Lambda}_t = \boldsymbol{\Lambda}_{t-1} \cup \{\lambda_t\}$ and $\mathbf{A}_t = [\mathbf{A}_{t-1} \boldsymbol{\alpha}_{\lambda_t}]$.
- 4) Solve a least square problem to obtain a new signal estimation:

$$\hat{\boldsymbol{\theta}}_{n,t} = \arg \min_{\boldsymbol{\theta}_t} \|\tilde{\mathbf{y}}_n - \mathbf{A}_t \boldsymbol{\theta}_t\|_2 = (\mathbf{A}_t^T \mathbf{A}_t)^{-1} \mathbf{A}_t^T \tilde{\mathbf{y}}_n \quad (12)$$

- 5) Calculate the new residual

$$\mathbf{r}_t = \tilde{\mathbf{y}}_n - \mathbf{A}_t \hat{\boldsymbol{\theta}}_{n,t} = \tilde{\mathbf{y}}_n - \mathbf{A}_t (\mathbf{A}_t^T \mathbf{A}_t)^{-1} \mathbf{A}_t^T \tilde{\mathbf{y}}_n \quad (13)$$

- 6) Increase t , and return to Step 2 if $t < k$.

2.3. Support Vector Machine

Support vector machines are supervised learning models with associated algorithms that analyze database on the idea of structural risk minimization. More formally, an SVM constructs a hyper-plane or set of hyper-planes in a high- or infinite-dimensional space. Usually, SVM can be used for classification, regression, or other tasks. SVM regression is usually referred to as support vector regression (SVR).

Consider a set of training data $\{(\mathbf{x}_1, z_1), \dots, (\mathbf{x}_l, z_l)\} \subset R^N \times R$ is given, where R^N denotes the space of input patterns. The idea of the regression problem is to determine a function that can approximate output values accurately. Therefore, we begin with describing the case of linear function f , which takes the form

$$z = f(\mathbf{x}) = \langle \mathbf{w}, \mathbf{x} \rangle + b \text{ with } \mathbf{w} \in R^N, b \in R \quad (14)$$

where $\langle \cdot, \cdot \rangle$ represents the dot product in R^N , and \mathbf{w} and b are unknown parameters obtained by minimizing the regression risk. One way to achieve minimal regression risk is to minimize the Euclidean norm $\|\mathbf{w}\|^2$. Then, the problem in Eq. (14) can be written as a convex optimization one:

$$\begin{aligned} \min \quad & \frac{1}{2} \|\mathbf{w}\|^2 \\ \text{s.t.} \quad & \begin{cases} z_i - \langle \mathbf{w}, \mathbf{x}_i \rangle - b \leq \varepsilon \\ \langle \mathbf{w}, \mathbf{x}_i \rangle + b - z_i \leq \varepsilon \end{cases} \end{aligned} \quad (15)$$

where ε is the precision of function f approximating all pairs of data (\mathbf{x}_i, z_i) .

Sometimes, some errors need to be allowed. We can introduce slack variables ξ_i, ξ_i^* to deal with the infeasible constraints of the optimization problem in Eq. (15). Then, the problem can be treated as follows

$$\begin{aligned} \min \quad & \frac{1}{2} \|\mathbf{w}\|^2 + C \sum_{i=1}^l (\xi_i + \xi_i^*) \\ \text{s.t.} \quad & \begin{cases} z_i - \langle \mathbf{w}, \mathbf{x}_i \rangle - b \leq \varepsilon + \xi_i \\ \langle \mathbf{w}, \mathbf{x}_i \rangle + b - z_i \leq \varepsilon + \xi_i^* \\ \xi_i, \xi_i^* \geq 0 \end{cases} \end{aligned} \quad (16)$$

The constant $C > 0$ is a tradeoff between the flatness of f and the amount of deviation allowed to be greater than ε . When the difference between the actual and estimated values is less than ε , it will be ignored. This formulation above can solve the problem of ε -insensitive loss function, taking the form

$$c(f(\mathbf{x}) - z) = \begin{cases} 0 & \text{if } |f(\mathbf{x}) - z| \leq \varepsilon \\ |f(\mathbf{x}) - z| - \varepsilon & \text{otherwise} \end{cases} \quad (17)$$

Since the relationship between the input and output is nonlinear, it can be implemented by transforming the training pattern \mathbf{x}_i into some feature space F , where there is a linear relationship between the input and output:

$$\begin{aligned} \phi : \mathbf{R}^N & \rightarrow F \\ \mathbf{x} & \rightarrow \phi(\mathbf{x}) \end{aligned} \quad (18)$$

The SVM algorithm relies on dot products between patterns \mathbf{x}_i , so the kernel function $k(\mathbf{x}, \mathbf{x}') = \langle \phi(\mathbf{x}), \phi(\mathbf{x}') \rangle$ is considered instead of ϕ to simplify the algorithm. To solve the above simplified optimization problem, we usually convert the primal problem to its dual one described as follows

$$\begin{aligned} \text{maximize} \quad & \begin{cases} -\frac{1}{2} \sum_{i,j=1}^l (\alpha_i - \alpha_i^*)(\alpha_j - \alpha_j^*) k(\mathbf{x}_i, \mathbf{x}_j) \\ -\varepsilon \sum_{i=1}^l (\alpha_i + \alpha_i^*) + \sum_{i=1}^l z_i (\alpha_i - \alpha_i^*) \end{cases} \\ \text{subject to} \quad & \sum_{i=1}^l (\alpha_i - \alpha_i^*) = 0 \quad \text{and} \quad \alpha_i, \alpha_i^* \in [0, C] \end{aligned} \quad (19)$$

The Lagrange multipliers α and α^* are calculated by solving the constrained quadratic programming problem (CQP). Then, function f can be given approximately by \tilde{f} :

$$\tilde{f}(\mathbf{x}) = \sum_{n=1}^{N_{sv}} (\alpha_n - \alpha_n^*) k(\mathbf{x}_n, \mathbf{x}) + b \tag{20}$$

where \mathbf{x}_n is the training pattern whose Lagrange multiplier is non-zero. This type of training pattern is called support vector (SV), and N_{sv} is the number of SVs.

In SVR, the kernel function is chosen as the Gaussian kernel and given by

$$k(\mathbf{x}_i, \mathbf{x}_j) = \exp(-\gamma \|\mathbf{x}_i - \mathbf{x}_j\|^2) \tag{21}$$

where γ is the variance of the kernel function. Before performing the SVR, some parameters such as C and γ need to be determined, which are adjusted using cross-validation during the training phase.

In the proposed method, \mathbf{x} represents the HRRP feature extracted from target backscattered signal, and z represents the x -coordinate or y -coordinate of the target position. After obtaining a set of pairs of \mathbf{x} and z , a nonlinear model between them can be achieved by training the dataset using SVR. Then, the position of the target is predicted through this nonlinear model. The whole procedure of the proposed method is shown in Fig. 1. In step 1, CS is applied to perform feature extraction of the target return received at each transceiver antenna position separately. In step 2, target detection is performed by using SVR model to predict the position of the target.

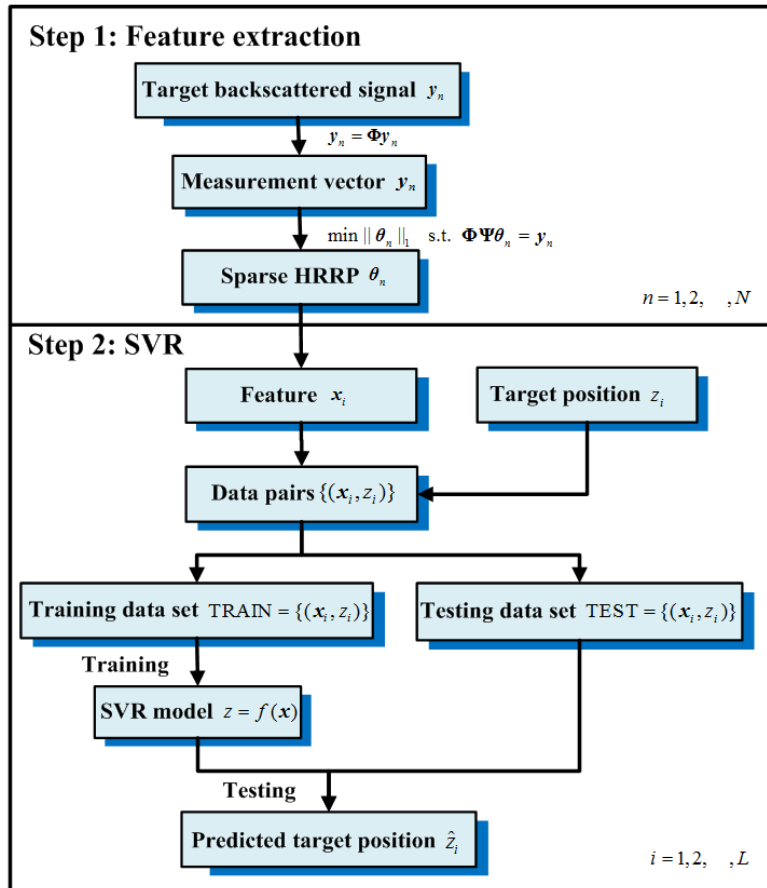


Figure 1. Procedure of the proposed method.

3. SIMULATION AND RESULTS

3.1. Simulation Model

In this section, the direct electromagnetic scattering is simulated to collect data. Fig. 2 shows the general situation of a metal target residing in a room with investigation domain $D = [-1.13, 1.13] \times [0.20, 3.70] \text{ m}^2$. The thickness, conductivity σ , and relative dielectric constant ϵ_r of the walls are 0.15 m, 0.003 S/m, and 7.66, respectively. The permeability of the walls is equal to μ_0 . SAR system is commonly used in through-wall imaging and detection. The transceiver TX/RX is 0.05 m away from the front wall and moves parallel to the wall to synthesize an aperture. The number of antenna positions is $N = 61$. The first antenna position is $(-1.2, 0) \text{ m}$, and the distance d between adjacent antenna positions is 0.04 m. The number of time samples at each antenna position is $M = 2000$. The electromagnetic field is obtained by performing finite difference time domain (FDTD) simulation. In FDTD simulation, the transmitted waveform at each antenna position is a sinusoidal modulated Gaussian pulse with a frequency of 2 GHz. The peak of the excitation pulse appears at $t_0 = 1.125 \text{ ns}$, and the spread of it is $\tau = 1.125 \text{ ns}$.

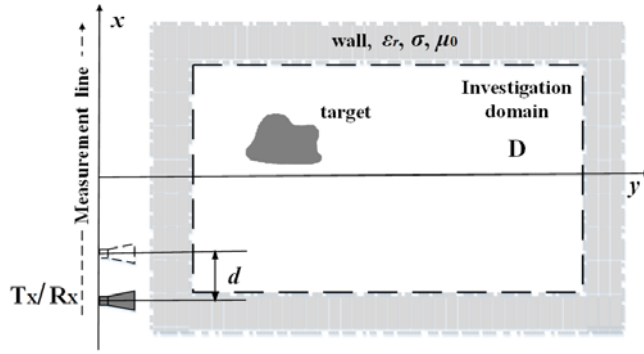


Figure 2. Simulation model of through-wall detection.

The original SAR data contain target echoes and wall reflections representing the main clutter source. For through-wall target detection, the target information is included in the target echo. In the following, signal \mathbf{y}_n refers to the one achieved by subtracting the background at the n th antenna position. The B-scan and A-scan of the target echo are shown in Fig. 3. Specifically, Fig. 3(a) exhibits the B-scan image of the target echo in which the target echo is marked out with a rectangle. Here, the target is located at $(0.03, 0.70) \text{ m}$. Fig. 3(b) shows the A-scan signal \mathbf{y}_{31} received at the 31th antenna position, which is marked with a black line in Fig. 3(a).

3.2. Feature Extraction and Target Detection

In the first part of this section, each sparse HRRP $\theta_n (n = 1, \dots, N)$ is recovered from the CS measurement $\tilde{\mathbf{y}}_n (n = 1, \dots, N)$ by solving the optimization problem in Eq. (10). Here, the measurement matrix Φ at all antenna positions are the same. All the elements are selected from the target signal $\mathbf{y}_n (n = 1, \dots, N)$, so the number of observations is $Q = M$. Assume that the detected scene (at each antenna position) is divided into $I = 91$ range cells when the range resolution $\Delta r = c/2B = 0.05 \text{ m}$ is guaranteed. Here, B is the bandwidth of the transmitted signal. The B-scan and A-scan of the sparse recovered HRRP are shown in Fig. 4. Fig. 4(a) shows the B-scan images of the sparse HRRP at all antenna positions when the target is located at $(0.03, 0.70) \text{ m}$. Here, the HRRP features are marked out with a red rectangle. Fig. 4(b) shows the A-scan of the sparse HRRP θ_{31} at the 31th antenna position, which is marked with a black line in Fig. 4(a). The results demonstrate that the target information for the target detection is contained in the sparse HRRP.

In the second part of this section, each largest value is extracted from the corresponding recovered HRRP to constitute a feature vector $\mathbf{x} \in R^N$, and then target detection is performed by using SVM

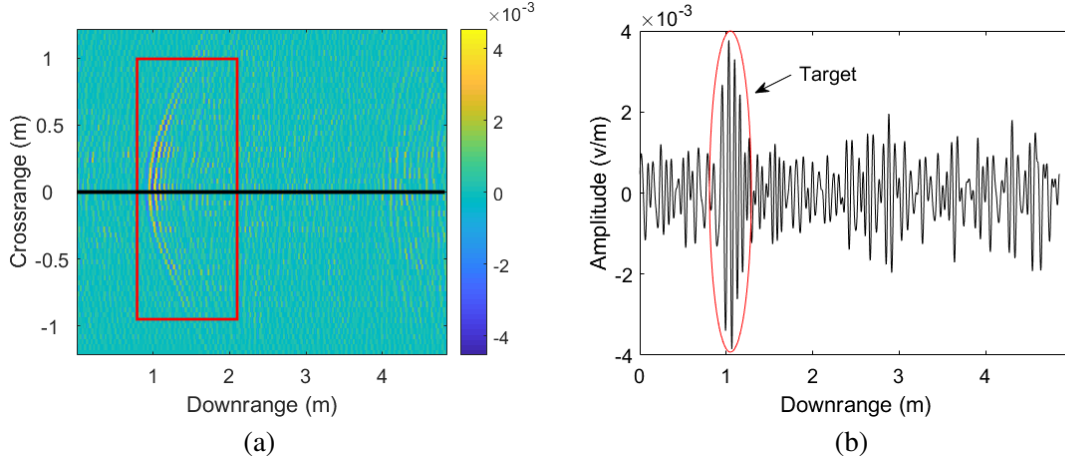


Figure 3. (a) B-scan image and (b) A-scan signal of the target echo received at the 31th transceiver antenna position.

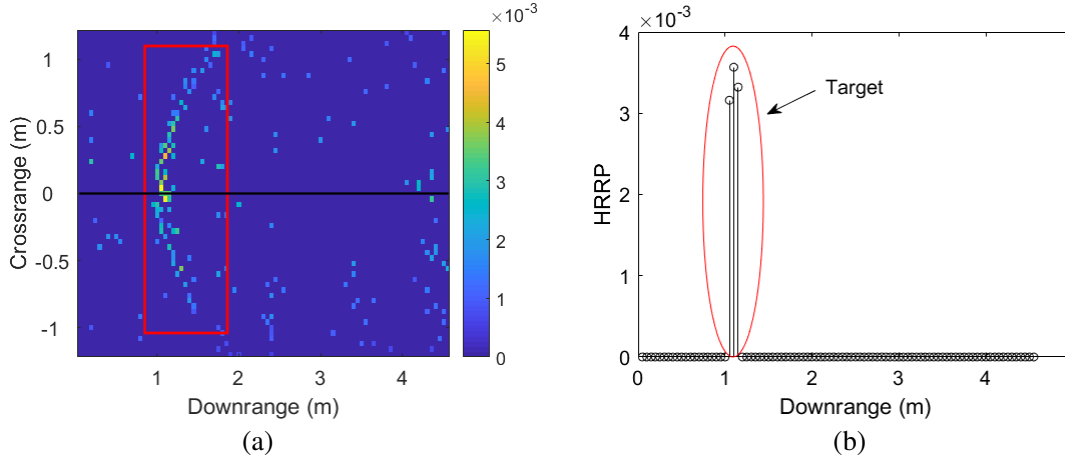


Figure 4. (a) B-scan image and (b) A-scan of the sparse HRRP at the 31th transceiver antenna position.

model to predict the position of the target. The feature vector \mathbf{x} is treated as the input of the SVM model, and the target position $z \in R$ is the output. A training data set $TRAIN = \{(\mathbf{x}_i, z_i), i = 1, 2, \dots, L\}$ including some input-output patterns is obtained with repeated simulations by changing the position of the target. Here, $L = 11 \times 17$ denotes the number of assumed target positions. For the training data set, the positions of the target are changed along the following way:

$$x_n = x_{0,\text{train}} + n\Delta x, \quad n = 0, 1, \dots, 10 \tag{22}$$

$$y_m = y_{0,\text{train}} + m\Delta y, \quad m = 0, 1, \dots, 16 \tag{23}$$

Here, $x_{0,\text{train}} = -0.97\text{m}$ is the initial x -coordinate of the target position, and $y_{0,\text{train}} = 0.3\text{m}$ is the initial y -coordinate of the target position. The spatial intervals in the x -axis and y -axis are $\Delta x = 0.2\text{m}$ and $\Delta y = 0.2\text{m}$, respectively. Given the training data set, the SVM model in Eq. (20) is obtained by solving the dual problem in Eq. (19).

To estimate the prediction accuracy of the SVM model, a test data set $TEST = \{(\mathbf{x}_i, z_i), i = 1, 2, \dots, L\}$ is generated. For the test data set, the positions of the target are changed in the following way:

$$x_n = x_{0,\text{test}} + n\Delta x, \quad n = 0, 1, \dots, 10 \tag{24}$$

$$y_m = y_{0,\text{test}} + m\Delta y, \quad m = 0, 1, \dots, 16 \tag{25}$$

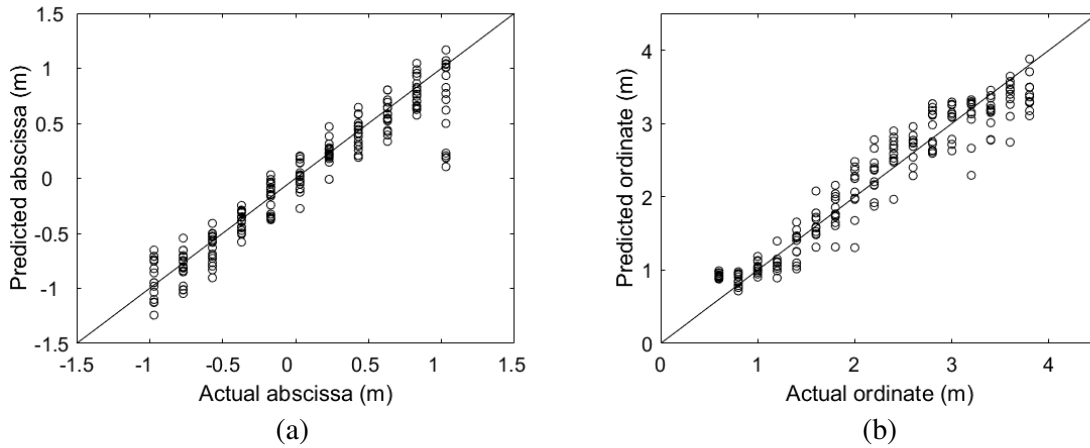


Figure 5. Predicted values of (a) the horizon and (b) depth of the target location versus the actual ones.

Here, $x_{0,\text{test}} = -1.03$ m and $y_{0,\text{test}} = 0.4$ m are the initial x -coordinate and y -coordinate of the target, respectively. Note that the test data set is different from the training data set since the assumed positions of the target are different in the two data sets. Firstly, we use the prediction results of horizon and depth of the target located in the enclosed room to demonstrate the effectiveness of the proposed method. Since the focus of evaluation is target detection, the constructed SVM model is first used to assess the degree of matching between the actual position and the predicted position composed of horizon and depth. The results are shown in Fig. 5, which shows that most of the predicted values are near the diagonal.

3.3. Analysis and Comparison

In this section, the effect of using different numbers of range cells on the detection accuracy is firstly analyzed. The number of range cells I is 91, 181, 271, 361, 451, 541, 631, 721, 811, and 901 when we set the size of range cell $\Delta r = 0.05$ m, 0.025 m, 0.0167 m, 0.0125 m, 0.01 m, 0.0067 m, 0.00625 m, 0.00556 m, and 0.005 m, respectively. The number of observations is still $Q = M$. In order to evaluate the proposed method quantitatively, the relative root-mean-square error (RMSE) of the prediction for horizon and

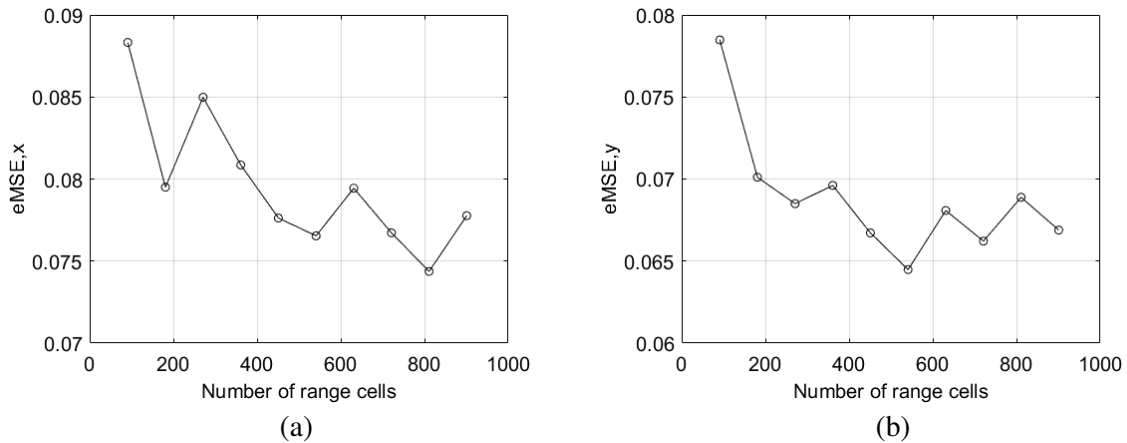


Figure 6. Prediction error vs. number of range cells for (a) the horizon and (b) depth of the target.

depth of the target location is defined as

$$e_{\text{RMS},x} = \sqrt{\frac{1}{L} \sum_{i=1}^L \left(\frac{x_i - \hat{x}_i}{l_x} \right)^2} \quad (26)$$

$$e_{\text{RMS},y} = \sqrt{\frac{1}{L} \sum_{i=1}^L \left(\frac{y_i - \hat{y}_i}{l_y} \right)^2} \quad (27)$$

Here (x_i, y_i) is the actual position of the target, and (\hat{x}_i, \hat{y}_i) is the predicted position of the target. $l_x = 2.26$ m and $l_y = 3.5$ m are the width and length of the room, respectively. The RMSEs versus different numbers of range cells are plotted in Fig. 6. It is obviously shown that the prediction error for either horizon or depth of the target decreases as the number of range cells increases. In general, the RMSE decreases at first and then decays more slowly afterwards. However, it is noted that the proposed method provides the lowest $e_{\text{RMS},x}$ when the number of range cells is 800 rather than 900 and the lowest $e_{\text{RMS},y}$ when the number of range cells is 500. The reason is that more range cells will result in a highly correlated sensing matrix in the framework of CS and thus a deteriorated detection performance.

Moreover, the effect of using different numbers of observations on the detection accuracy is also analyzed. Assume $I = 91$ as the number of range cells. Data are measured with 10%, ... 100% of the full measurements received at each antenna position randomly. Hence, the number of observations is $Q = 10\%M, \dots, Q = 100\%M$. Each simulation is repeated 100 times, and the average results are reported in Fig. 7. It can be seen from Figs. 7(a) and (b) that larger number of observations results in lower RMSE. To achieve higher detection accuracy, e.g., $e_{\text{RMS},x} < 0.085$ (or $e_{\text{RMS},y} < 0.085$), at least 50% of full measurement data need to be acquired for the recovery of the HRRP when CS algorithm is used.

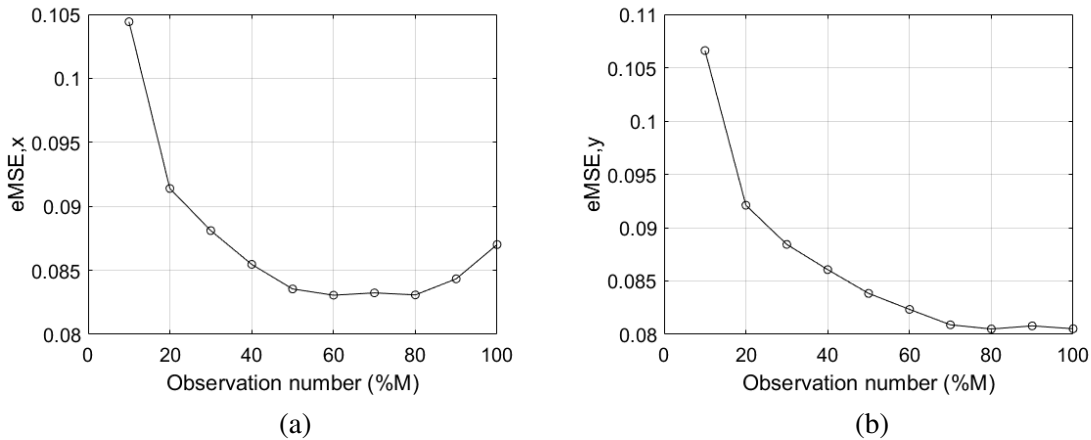


Figure 7. Prediction error vs. number of observations for (a) the target abscissas and (b) target ordinates.

Finally, the comparison between the method in which we use amplitude of the target signal as a feature and the method in which CS is performed to extract HRRP feature is carried out. Meanwhile, the prediction error with respect to the noise level is analyzed. In this experiment, the number of observations is set to $Q = 40\%M$ and $Q = 80\%M$, and the number of range cells I is set to 91 and 451, respectively. Each simulation is repeated 100 times, and the average results are illustrated in Fig. 8. The results also demonstrate that larger number of observations Q (or number of range cells I) will result in lower RMSE, and the proposed method has smaller RMSE of the prediction. Moreover, the results indicate that better robustness of the proposed method is obtained with noisy input data.

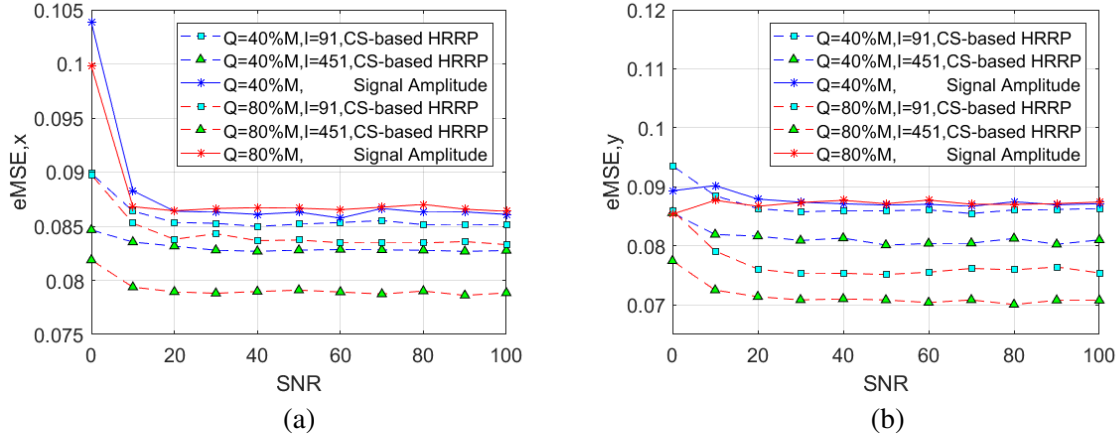


Figure 8. Prediction error vs. SNR for (a) the horizon and (b) depth of the target.

4. CONCLUSION

In this paper, the feature HRRP which is extracted based on CS algorithm is incorporated into an SVM regression procedure to obtain high accuracy target detection through the wall. Due to the sparsity of the HRRP, it can be recovered from low dimensional measurements by solving a norm-minimization problem. Then, target detection is performed by using SVM model to predict the position of the target with the feature HRRP being treated as input and the target position as output. The results not only validate the accuracy of the proposed method, but also show its high efficiency. The results demonstrate that the prediction accuracy of target position is related to the number of range cells, the number of observations, and SNR. Simulation results also show that the proposed method has smaller RMSE and better robustness than the one in which signal amplitude is treated as a feature.

ACKNOWLEDGMENT

We want to thank the helpful comments and suggestions from the anonymous reviewers. This work was supported by the National Natural Science Foundation of China (Grant No. 61601245 61601242), and State Key Laboratory of Millimeter Waves Open Project, Southeast University (Grant No. K201724), China Postdoctoral Science Foundation Funded Project (Grant No. 2016M601693) and Nanjing University of Posts and Telecommunications Foundation, China (Grant No. NY214047).

REFERENCES

1. Sun, S., B. J. Kooij, and A. G. Yarovoy, "Linearized 3-D electromagnetic contrast source inversion and its applications to half-space configurations," *IEEE Transactions on Geoscience and Remote Sensing*, Vol. 55, 3475–3487, Jun. 2017.
2. Lu, B. Y., Q. Song, Z. M. Zhou, and X. Zhang, "Detection of human beings in motion behind the wall using SAR interferogram," *IEEE Geoscience and Remote Sensing Letters*, Vol. 9, 968–971, Sep. 2012.
3. Li, H. Q., G. L. Cui, L. J. Kong, G. H. Chen, M. Y. Wang, and S. S. Guo, "Robust human targets tracking for MIMO through-wall radar via multi-algorithm fusion," *IEEE Journal of Selected Topics in Applied Earth Observations and Remote Sensing*, Vol. 12, 1154–1164, Apr. 2019.
4. Guo, S. S., G. L. Cui, L. J. Kong, and X. B. Yang, "An imaging dictionary based multipath suppression algorithm for through-wall radar imaging," *IEEE Transactions on Aerospace and Electronic Systems*, Vol. 54, 269–283, Feb. 2018.

5. Qu, L. L., X. Cheng, Y. P. Sun, and T. H. Yang, "Compressive sensing-based two-dimensional diffraction tomographic algorithm for through-the-wall radar imaging," *2018 Progress In Electromagnetics Research Symposium (PIERS — Toyama)*, 2384–2388, Japan, Aug. 1–4, 2018.
6. Wang, F. F., Y. R. Zhang, and H. M. Zhang, "Joint wall clutter mitigation and data-driven model for through-wall detection," *International Journal of Remote Sensing*, Vol. 37, 4486–4499, 2016.
7. Wang, F. F., Y. R. Zhang, and H. M. Zhang, "Through-wall detection with LS-SVM under unknown wall characteristics," *International Journal of Antennas and Propagation*, 2016.
8. Du, L., P. H. Wang, H. W. Liu, M. Pan, F. Chen, and Z. Bao, "Bayesian spatiotemporal multitask learning for radar HRRP target recognition," *IEEE Transactions on Signal Processing*, Vol. 59, 3182–3196, Jul. 2011.
9. Du, C., B. Chen, B. Xu, D. D. Guo, and H. W. Liu, "Factorized discriminative conditional variational auto-encoder for radar HRRP target recognition," *Signal Processing*, Vol. 158, 176–189, May 2019.
10. Zheng, C., G. Li, X. G. Xia, and X. Wang, "Weighted $l(2,1)$ minimisation for high resolution range profile with stepped frequency radar," *Electronics Letters*, Vol. 48, 1155–U190, Aug. 30, 2012.
11. Li, H. T., C. Y. Wang, K. Wang, Y. P. He, and X. H. Zhu, "High resolution range profile of compressive sensing radar with low computational complexity," *IET Radar Sonar and Navigation*, Vol. 9, 984–990, Oct. 2015.
12. Yang, L., L. F. Zhao, S. Zhou, and G. A. Bi, "Sparsity-driven SAR imaging for highly maneuvering ground target by the combination of time-frequency analysis and parametric Bayesian learning," *IEEE Journal of Selected Topics in Applied Earth Observations and Remote Sensing*, Vol. 10, 1443–1455, Apr. 2017.
13. Baraniuk, R. G., "Compressive sensing," *IEEE Signal Processing Magazine*, Vol. 24, 118, Jul. 2007.
14. Candes, E. J. and M. B. Wakin, "An introduction to compressive sampling," *IEEE Signal Processing Magazine*, Vol. 25, 21–30, Mar. 2008.
15. Tropp, J. A. and A. C. Gilbert, "Signal recovery from random measurements via orthogonal matching pursuit," *IEEE Transactions on Information Theory*, Vol. 53, 4655–4666, Dec. 2007.